International Journal of Microwave and Wireless Technologies

cambridge.org/mrf

Circular polarized two-element textile antenna with high isolation and polarization diversity for wearable applications

Anubhav Kumar[1], Asok De[2] and R. K. Jain[1]

[1]Department of Electronics and Communication Engineering, Shobhit Institute of Engineering and Technology, (Deemed to be University), Meerut, Uttar Pradesh, India and [2]Delhi Technological University (DTU), New Delhi, India

Research Paper

Cite this article: Kumar A, De A, Jain RK (2023). Circular polarized two-element textile antenna with high isolation and polarization diversity for wearable applications. *International Journal of Microwave and Wireless Technologies* **15**, 493–501. https://doi.org/10.1017/S1759078722000332

Received: 18 May 2021
Revised: 16 February 2022
Accepted: 19 February 2022
First published online: 14 March 2022

Keywords:
5 G communications; circularly polarized antenna; multi-input and multi-output (MIMO) antenna; wearable application

Author for correspondence:
Anubhav Kumar,
E-mail: rajput.anubhav@gmail.com

Abstract

A two-element textile antenna with high isolation and polarization diversity is presented for 5 G communications, wearable technology and biomedical cancer detection applications. The flexible material is used with an orthogonally placed microstrip-feed radiator antenna responsible for polarization diversity. High isolation and low correlation are achieved between antenna elements with defected ground-based on diagonal and open-stubs, which perturbs the surface current and facilitates the achievement of circular polarization. The 10 dB impedance bandwidth ($|S_{11}|$) of a two-element antenna varies from 3.3 to 4.3 GHz with more than 24 dB isolation ($|S_{21}|$). The envelope correlation coefficient (ECC) and channel capacity loss (CCL) of multi-input and multi-output (MIMO) antenna parameters are less than 0.2 and 0.35 bits/s/Hz respectively, which validates the diversity performance of the antenna.

Introduction

Applications of flexible antennas have been increasing in recent wireless communication technology, therefore, these antennas are required for communication applications in portable devices, gadgets, smart clothes, microwave imaging, real-time health monitoring, biomedical, sports, and short-distance communication from one device to another [1]. The compact and wearable antenna is preferred to establish connectivity in portable devices to enhance life efficiency and real-time monitoring as well as internet connectivity between devices and sensors. Textile substrate antennas are a strong choice due to low cost, flexibility, and easy inclusion in wearable devices as well as fabrication in the garment. The wireless system requires a multi-input and multi-output (MIMO) antenna with recently introduced 5G communication and increased demand for data rate and channel capacity, while the antenna also will further increase the channel capacity of the system if it is circularly polarized [2]. Although designing a MIMO antenna for wearable gadgets is a challenging problem in itself but it is very important for wearable devices to have a compact antenna with minimum distance between antenna elements in the limited space, this increases the mutual coupling, which affects the antenna performance [3].

In the literature, many single-element [4–6] and two-element antenna [7–12] designs are studied for wearable and biomedical applications with textile or flexible material. In [4], a dual-band, s-shaped single element textile antenna with co-axial feed based on two open stubs in the ground is used for ISM band and on-body communication. In [5], E-shaped etched on the rectangular radiator with the partial ground using textile material for ISM and medical communication is presented. In [6], flexible and single element, fractal microstrip antenna with the defected ground and a meandering line is designed for ISM bands and on-body applications, where size miniaturization and bandwidth enhancement is achieved. The MIMO antenna fulfills the requirement of present communications but the demand of compact size is a complex approach as antenna edge to edge distance affects the correlation and isolation which in-turn affects the MIMO antenna performance. Many complex decoupling technologies are discussed in the literature to diminish the surface current moving from one port to another port and improve the isolation. A two-element antenna with the rectangular-shaped radiator is accomplished on jeans material with partial ground [7], where I-shaped decoupling structure diminished the surface current and reduced the mutual coupling between antenna elements. In [8], a switch-based reconfigurable MIMO antenna with the partial defected ground is used which can be applicable on wideband frequencies and wearable applications. In [9], the two-element textile antenna is designed for medical and wearable communication, where T-shaped with three rings decoupling structure enhanced the isolation between antenna elements. In [10], a two-element antenna based on the dual-ring shaped radiator for UWB wearable application is used where isolation between elements is improved with two symmetric inverted U-shaped decoupling structures in the ground. In [11], open-stub is etched in the rectangular radiator to achieve the ISM band, where the unconnected ground is used in a two-element flexible

CAMBRIDGE UNIVERSITY PRESS

antenna and an inverted U-shaped parasitic stub is used to diminish the mutual coupling. In [12], the dual-polarized two-element textile antenna is used with a meander-line decoupling structure for wearable applications. In [13], a single element planer antenna is designed for dual-band wearable applications. In [14], CPW-fed monopole antenna is designed with circular ground and Kapton substrate for multiband wireless communication applications. In the above discussion, it is revealed that to reduce the mutual coupling in the textiles or wearable MIMO antenna, where port isolation is increased by increasing the distance between the two elements as well as by unconnected ground, thereby increasing the size of the antenna.

However, in wearable applications, it is considered more effective to minimize the effective area of the antenna, so that the antenna can be easily embedded in the working space and reduce its space by incorporating battery and sensors in the devices. Antenna elements are placed orthogonally and in a different plane to keep the compact size, less complexity in MIMO antenna with high isolation ($|S_{21}|$), which can be easily accomplished in any device. In portable and wearable applications the direction of EM waves is not fixed as devices can change the physical position with time in this case, the polarization diversity improves the performance of the MIMO antenna and receives the EM waves from different directions. MIMO antenna also fulfills the present and future wearable and portable application where more than one sensor is used therefore multiple signals can be transmitted and received at the same time. Circular polarized (CP) MIMO antennas improve the MIMO antenna performance and improve the channel capacity in a multipath environment over the linear polarized (LP) antenna [2]. This two-element antenna is designed for wearable and biomedical application at 5G communication, where the novelty and major technical contributions are discussed below:

(1) The two-element antenna is designed on low-cost and flexible textile jeans material.
(2) The two-element antenna is designed for 5G communication, wearable technology and biomedical applications for 3.3 to 4.3 GHz.
(3) Both two elements radiate LHCP/RHCP waves in the entire operating band whereas it helps to improve the channel capacity of the system when compared to LP antenna [2].
(4) The antenna step-feed is placed orthogonal and it provides the diversity performance as well as receives and radiates the EM waves from different directions.
(5) Open-stubs and diagonal strips play an important role to obtain the CP waves and improve the isolation ($|S_{21}|$) between antenna elements, which is more than 24 dB.
(6) The two-element antenna is analyzed on a human female breast model, which provides the SAR values for the detection of malignant tissues.

In this paper, a two-element textile diversity/MIMO antenna is designed with step-feed, open-stubs, and diagonal stub in the ground for isolation enrichment, where 3.3 to 4.3 GHz operating bandwidth ($|S_{11}|$) is achieved with isolation ($|S_{21}|$) more than 24 dB and left-hand circular polarization (LHCP) and right-hand circular polarization (RHCP) in the entire operating band. The proposed two-port CP diversity antenna is designed to be part of the wearable application, covering the frequency band of 5G communication with high port isolation ($|S_{21}|$) on flexible material, diversity performance, low envelope correlation coefficient (ECC) with circular polarization in the entire operating band.

Design of two-element antenna

The proposed two-element, textile, CP antenna and its fabricated prototype are represented in Figs 1(a) and 1(b).

The copper tape of 0.057 mm thickness is used as a conducting element whereas jeans material (loss tangent ($\tan\delta$) = 0.025) with permittivity (ε_r) of 1.7 and thickness (t) of 1 mm is used as a substrate. The width (W_s) and length (L_s) of the substrate are 31 × 31 mm^2. The dimensions of the circularly polarized textile antenna are depicted in Table 1. The proposed antenna evolution is discussed in five steps, which are illustrated in Fig. 1(c). In step-1, two orthogonally placed microstrip step-feed is accomplished with the defected ground. The impedance bandwidth ($|S_{11}|$) and isolation ($|S_{21}|$) are achieved from 3.2 to 4.8 GHz and 11 to 15 dB respectively, as depicted in Figs 1(d) and 1(e). In step-2, width W1 is increased with symmetrically open stub on both sides in the ground, which perturbs the surface current in the ground and supports circular polarization. The axial ratio in Fig. 1(f) reveals that the width (W1) and open stub in the ground shift the axial ratio in the operating band close to 3 dB whereas it is less than 3 dB at 3.2 GHz. The impedance bandwidth ($|S_{11}|$) varies from 3.6 to 4.4 GHz in this step with isolation ($|S_{21}|$) more than 13.5 dB. In step-3, a diagonal stub is accomplished in the ground to diminish the surface current between ports, which improves more than 5 dB isolation ($|S_{21}|$) along with axial ratio as illustrated in Fig. 1(f). The impedance bandwidth ($|S_{11}|$) of the antenna is achieved from 3.3 to 4.3 GHz with isolation ($|S_{21}|$) more than 18.5 dB. In step-4, two symmetric L-shaped open-stubs are incorporated between the ports to further enhance the isolation ($|S_{21}|$) and axial ratio. The impedance bandwidth ($|S_{11}|$) is obtained from 3.4 to 4.4 GHz with 18.4 to 21.9 dB isolation. In step-5, impedance matching is enhanced with a rectangular slot introduced in the ground behind the step feed, which improves the impedance bandwidth ($|S_{11}|$) and isolation ($|S_{21}|$) of the two-element antenna. The impedance bandwidth ($|S_{11}|$) of the antenna varies from 3.3 to 4.3 GHz with more than 24 dB isolation and the less than 3 dB axial ratio is achieved in the entire operating band.

Analysis of circular polarization and surface current of two-element antenna

In this section, axial ratio, surface current and radiation characteristics are analyzed to understand the antenna performance. It is clear from the previous section that the defected ground with open-stubs as well as the position of feed perturbs the surface current, which enhances the isolation ($|S_{21}|$) and axial ratio (dB) for achieving the CP band. The obtained 3 dB axial ratio covers the entire operating band. The vector analysis of surface current is investigated at 0°, 90°, 270° and 360° phase in 3.8 GHz as depicted in Fig. 2(a). It is revealed that the direction of the current vectors in the ground is clockwise as well as anti-clockwise which validates LHCP and RHCP in the antenna. The surface current at 3.8 GHz in port-1 is excited and is represented in Fig. 2(b), where the open-stubs mitigate the surface current moving from one port to another in a clockwise and anti-clockwise direction, which improves the isolation ($|S_{21}|$), and reduce the mutual coupling of the antenna. The 3D radiation pattern at 3.8 GHz is illustrated in Fig. 2(c), the figure reveals the diversity performance of the two-port antenna and its ability to transmit and receive the EM waves from different directions.

https://doi.org/10.1017/S1759078722000332 Published online by Cambridge University Press

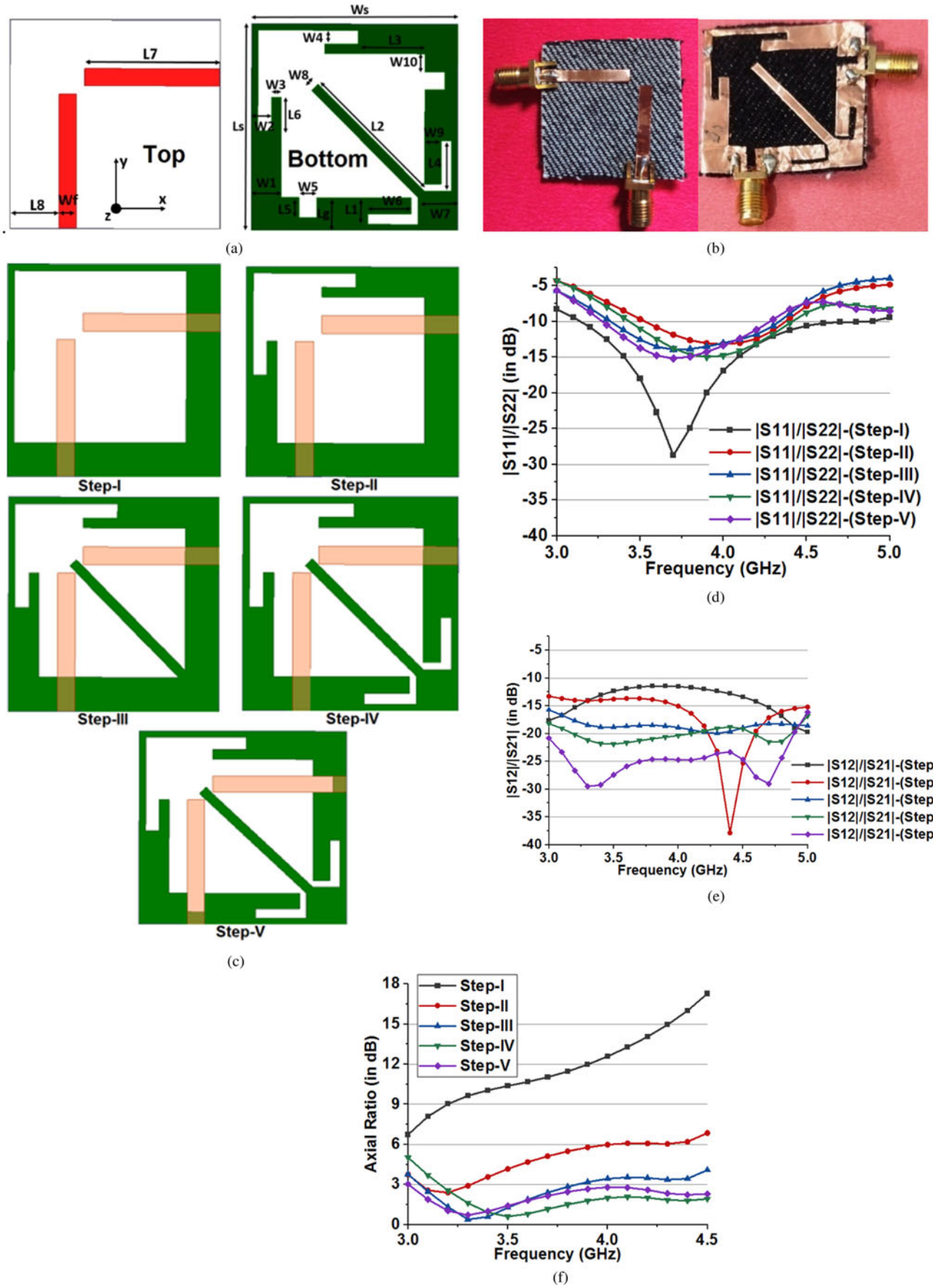

Fig. 1. Textile two-element antenna (a) prototype design (b) hardware (c) design steps (d) $|S_{11}|/|S_{22}|$ of design steps (e) $|S_{12}|/|S_{21}|$ of design steps (f) axial ratio (dB) in different steps.

https://doi.org/10.1017/S1759078722000332 Published online by Cambridge University Press

Table 1. Dimensions of different geometrical parameters

Parameter	Ls	Ws	W1	L1	W2	L2
Values (mm)	31	31	4.5	4	3	22.627
Parameter	W3	L3	W4	L4	W5	L5
Values (mm)	1.5	10	2	6.5	2.6	3
Parameter	W6	L6	W7	L7	W8	L8
Values (mm)	6.5	5	6	20	1.414	7.2
Parameter	W9	Wf	W10			
Values (mm)	2.5	2.6	2.7			

Simulated and experiment results

The CP and two-element antenna is measured on Anritsu MS2025B VNA to verify the simulation results obtained from HFSS 13.

The 10 dB impedance bandwidth ($|S_{11}|$) varies from 3.3 to 4.3 GHz while the isolation ($|S_{21}|$) is more than 24 dB as depicted in Fig. 3(a), where the measured results are close to simulated results that validate the results. A minor deviation is found between simulated and measured results due to some irregularities in soldering and fabrication. The realized gain (dB) of the antenna varies from 3 to 3.45 dB and less than 0.5 dB gain variation is achieved in all operating bandwidths as illustrated in Fig. 3(b). The axial ratio (3 dB) is illustrated in Fig. 3(c), which reveals that less than 3 dB measurement and simulated results are achieved. The measured and simulated E and H components (radiation pattern) of an antenna are 90 degrees out of phase at 0°, 90°, 180° and 270° degree which validates the circular polarization behavior of the antenna. The radiation efficiency (%) is achieved more than 90 in the entire operating band. In this paper, equation (1) is used to calculate the transmission efficiency [13] of the proposed CP antenna where the Tx antenna or Rx antenna is analyzed with a variation of 10 mm over a distance of 10 to 50 mm at 3.8 GHz. The analysis of transmission

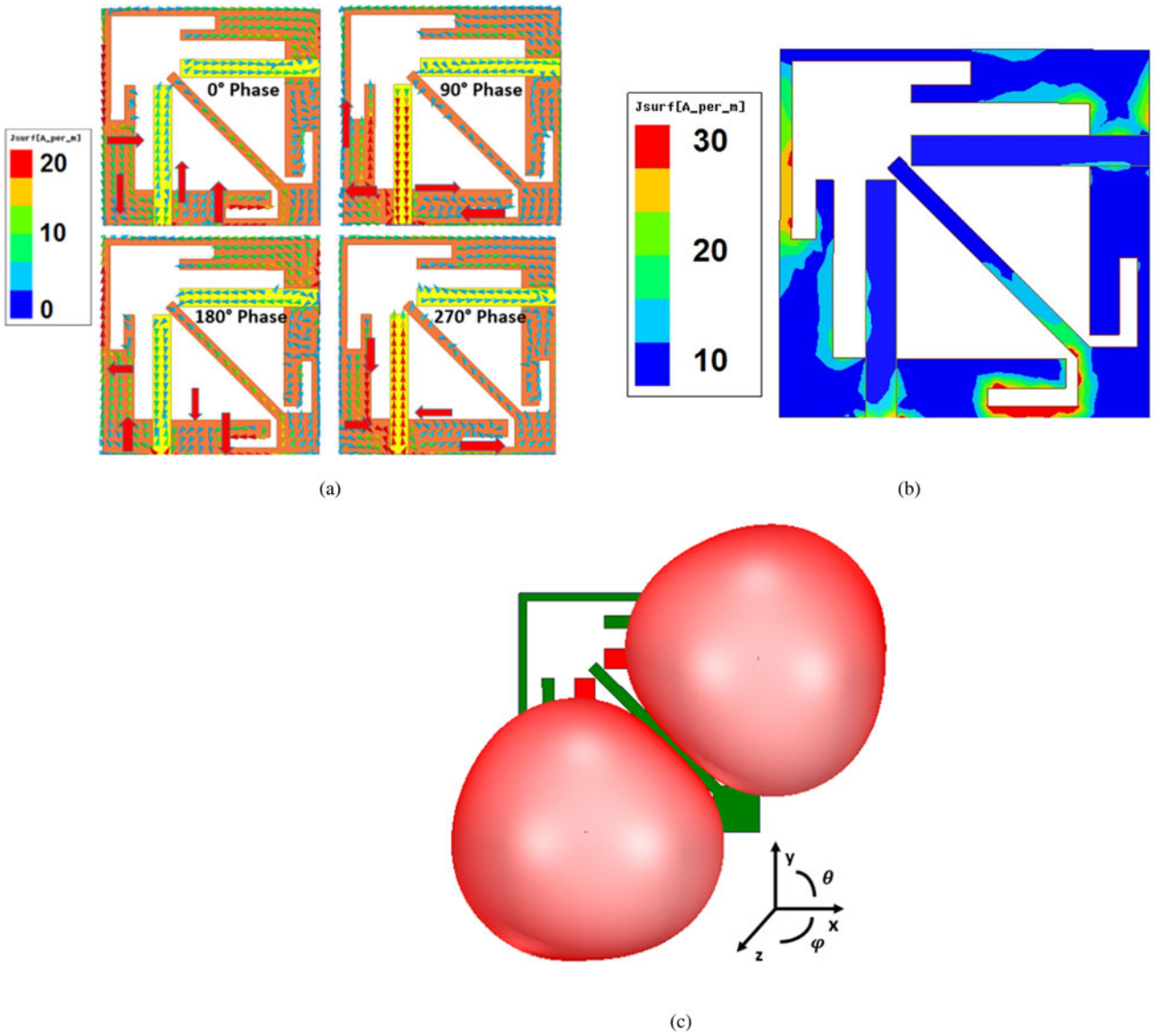

Fig. 2. Textile two-element diversity antenna (a) CP behaviors analysis form surface current (b) surface current when port-1 is excited (c) 3D radiation pattern.

https://doi.org/10.1017/S1759078722000332 Published online by Cambridge University Press

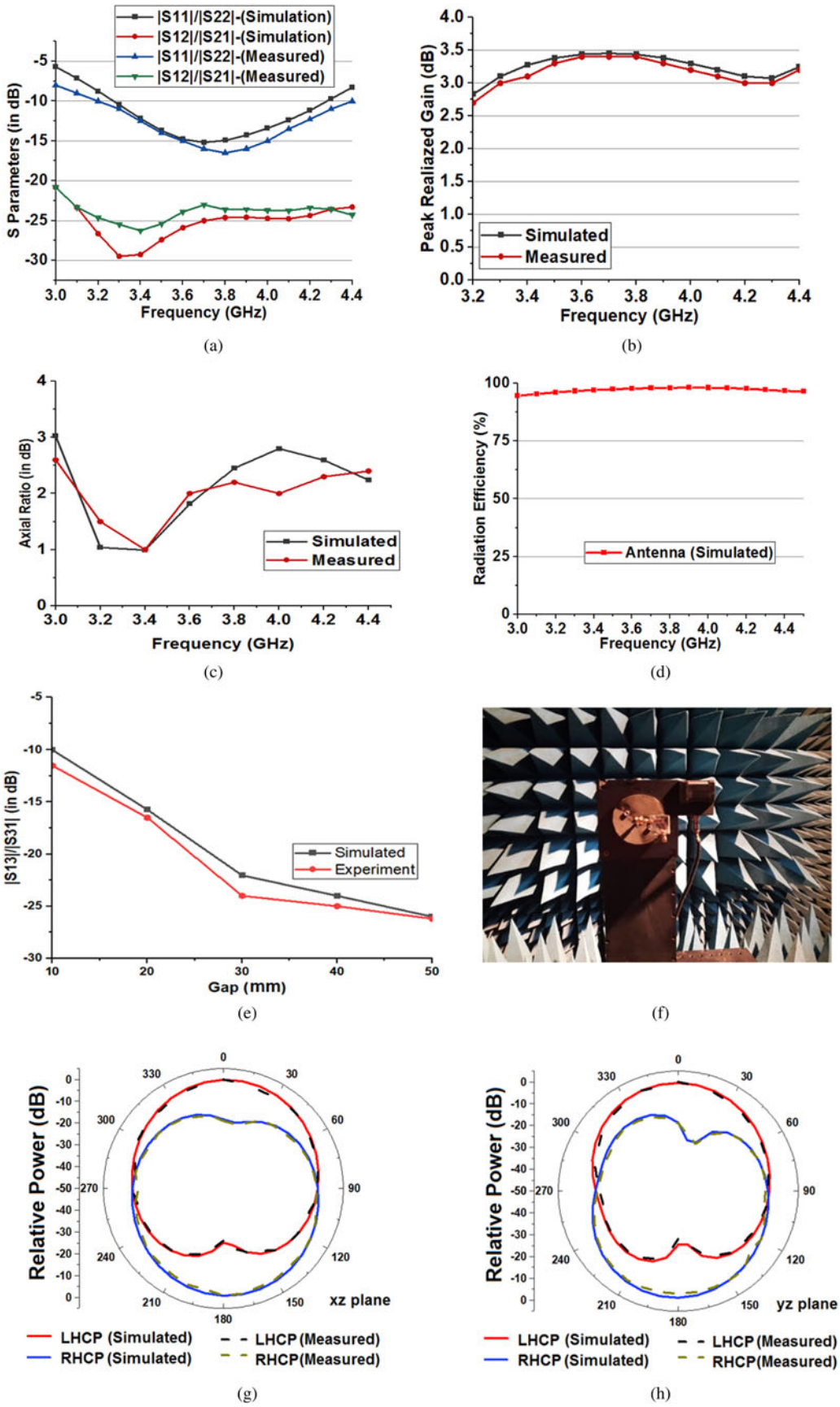

Fig. 3. Textile two-element diversity antenna (a) simulated and measured s-parameters (b) realized gain (dB) (c) axial ratio (dB) (d) radiation efficiency (%)(e) Transmission coefficient (S_{21}) at 3.7 GHz with Rx antenna distance varies from 10 to 50 mm (f) Measurement set-up (g) and (h) normalized radiation pattern at 3.8 GHz (i) Measurement of antenna on the human body (j) $|S_{11}|$ and $|S_{12}|$ analysis of antenna on the human body (Simulated and measured).

https://doi.org/10.1017/S1759078722000332 Published online by Cambridge University Press

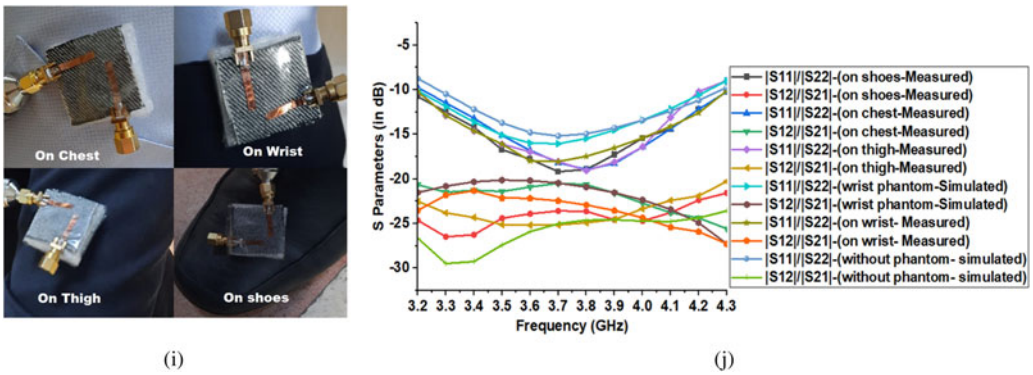

Fig. 3. Continued.

coefficient ($|S_{31}|$) in dB at different distances is shown in Fig. 3(e). The Antenna-1 is the Tx antenna and Antenna-3 is the Rx antenna because the Antenna-1 and antenna-2 are accomplished in transmitter antenna where in Ref [13] paper, Antenna-1 is the transmitter and antenna-2 is the Rx antenna. The fractional variation of transmission efficiency from 10to 50 mm is 2.94% while for 20 to 50 mm is 11.3%, which makes it appear that the antenna can work effectively with minimum variation in transmission efficiency.

$$\eta = (|S_{31}|^2) \times 100\% \tag{1}$$

In design, both antenna elements are the same, therefore measurement is done in Ant-1 and another element is terminated with a matched load of 50 Ω in an anechoic chamber where the distance from reference antenna to under test antenna is 3 meter as depicted in Fig. 3(f), ridge type horn antenna used as a reference antenna with more than 11 dB gain at operating bandwidth. The LHCP and RHCP normalized radiation patterns at 3.8 GHz in the xz and yz planes are illustrated in Figs 3(g) and 3(h), where a stable radiation pattern is observed.

The two-port antenna is analyzed on the chest, wrist, thigh and shoes at 20 mm distance from the antenna where foam padding is used to separate the antenna from the human body which does not affect the s-parameter as depicted in Fig. 3(i). The simulation analysis is conducted on the human wrist phantom model. The electrical characteristics of the human wrist phantom model is taken from Ref [15] and the thickness of skin, fat, and muscle are used 2, 5, and 10 mm with 50 mm × 50 mm dimensions. The distance of the phantom model from an antenna is 20 mm to remove the coupling effect as well as a minimum effect on the isolation of the antenna. The measured and simulated results of $|S_{11}|$ and $|S_{12}|$ parameters are illustrated in Fig. 3(j), where small variation is found in impedance bandwidth ($|S_{11}|$) and isolation is higher than 20 dB in all on-body measurements. The antenna elements are orthogonally placed in the design; therefore, the antenna provides the pattern diversity, which can be observed from the radiation patterns. The diversity performance of the antenna is also determined from the MIMO parameters, therefore ECC and diversity gain (DG) are analyzed with radiation pattern from equations (2) to (3) [16] whereas total active reflection coefficient (TARC) and channel capacity loss (CCL) are extracted from the simulated and measured s-parameter and computed from equations (4) to (5) [3].

$$ECC = \frac{\left|\left(\int_0^{2\pi}\int_0^{\pi}(XPR\,E_{\theta 1}E^*_{\theta 2}P_\theta + E_{\varphi 1}E^*_{\varphi 2}P_\varphi)\right)\mathrm{Sin}\theta d\theta d\varphi\right|^2}{\int_0^{2\pi}\int_0^{\pi}\left(XPR\,E_{\theta 1}E^*_{\theta 1}P_\theta + E_{\varphi 1}E^*_{\varphi 1}P_\varphi\right)\mathrm{Sin}\theta d\theta d\varphi \times \int_0^{2\pi}\int_0^{\pi}\left(XPR\,E_{\theta 2}E^*_{\theta 2}P_\theta + E_{\varphi 2}E^*_{\varphi 2}P_\varphi\right)\mathrm{Sin}\theta d\theta d\varphi} \tag{2}$$

$$DG = 10\sqrt{1 - |ECC|^2} \tag{3}$$

$$TARC = \frac{\sqrt{(|S_{11} + S_{12}e^{j\theta}|^2 + |S_{22}e^{j\theta} + S_{21}|^2)}}{\sqrt{2}} \tag{4}$$

$$CCL = -\log_2 \det(\psi^R) \tag{5}$$

The ECC represents a correlation of the radiation pattern of antenna elements and its practical accepted value should be less than 0.5 where DG should be higher for practical applications. The extracted simulated and measured ECC and DG is < 0.2 and close to 10 dB respectively, therefore good diversity performance of the two-port textile antenna is achieved as depicted in Figs 4(a) and 4(b). The TARC and CCL of MIMO antenna parameters are extracted from equations (3) and (4), where the correlation matrix at receiving end is represented by ψ^R. The results reveal that the minimum variation is observed in the measured value of the TARC at different phase angles whereas measured and simulated CCL is less than 0.35 bits/sec/Hz in the entire operating band (Figs 4(c) and 4(d)). The CCL is less than the accepted value of 0.4 bits/sec/Hz [3]. Table 2 represents the comparative analysis with recently published textile or flexible single element and two-element antenna. The analysis reveals that the proposed antenna is compact, low cost and flexible with low ECC. The diversity performance and CP is achieved in the entire operating band, however, it can be a good candidate for the 5G, wearable and biomedical applications.

Simulated analysis of breast cancer detection

In this section, simulation analysis is investigated on the human female breast model and standard parameters of skin, fat, glandular tissue, as well as a tumor cell, are used [15]. The proposed

https://doi.org/10.1017/S1759078722000332 Published online by Cambridge University Press

Table 2. Comparison analysis of proposed antenna with existing antenna

Reference	No of elements	Size	Material	Bandwidth (GHz)	Isolation	ECC	CP
[4]	1	60 × 30	Felt	2.45 and 5.8	NA	NA	No
[5]	1	30 × 20	Denim	2.4	NA	NA	No
[6]	1	39 × 39	Rogers 5880	2.36–2.55	NA	NA	No
[7]	2	40 × 70	Jeans	2.4–8.0	>22	<0.01	No
[8]	2	35 × 30	Jeans	3.11–5.15, 4.81–7.39	>19.5, 21	< 0.18	No
[9]	2	76 × 37	Felt	2.00–6.23	>29.26	<0.01	No
[10]	2	50 × 35	Jeans	1.83–13.82	>21 dB	<0.39	No
[11]	2	28 × 25	Rogers 5880	2.45	>30	0.025	No
[13]	1	15 × 14	Kapton polyimide	2.5 /4.5	NA	NA	No
[14]	1	70 × 70	Kapton substrate	1.2, 2.0, 2.6 and 3.4	NA	NA	No
Proposed	2	31 × 31	Jeans	3.3 to 4.3	>24	<0.2	Yes

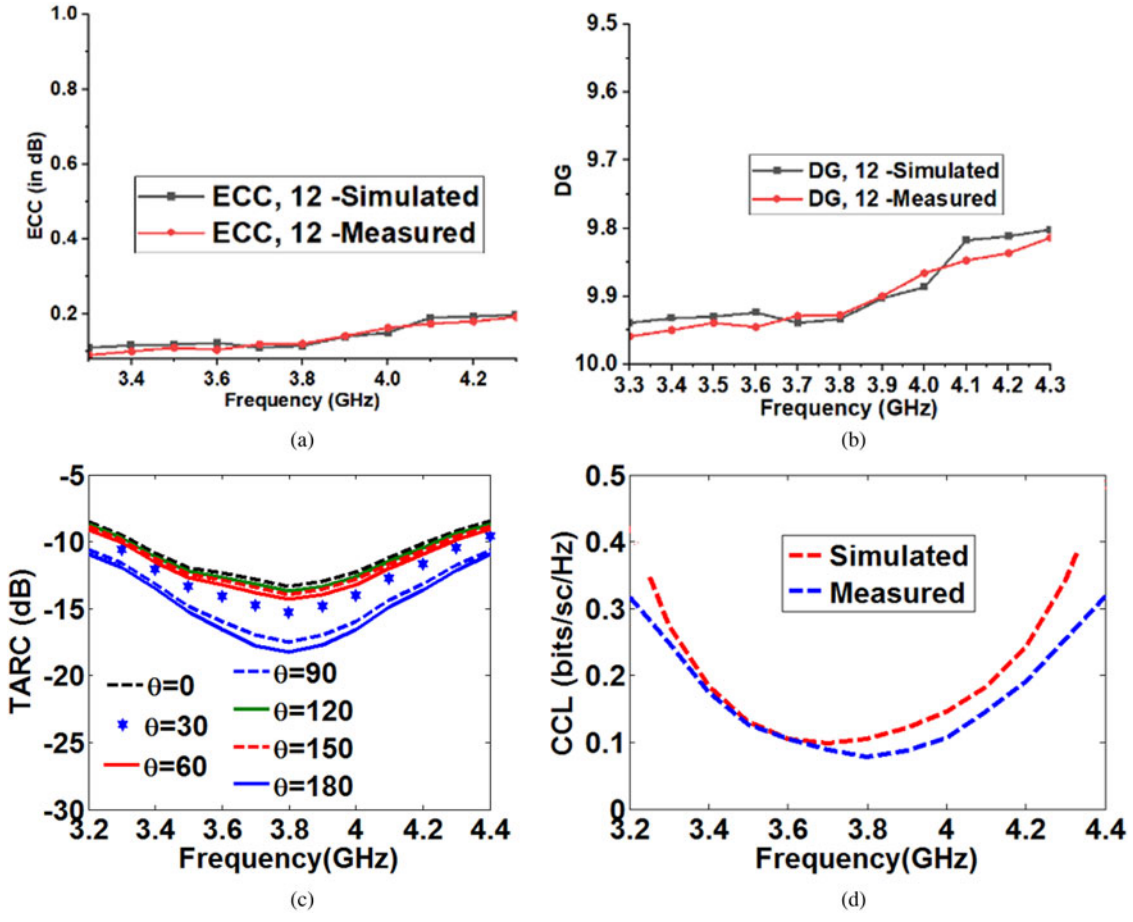

Fig. 4. Textile two-element diversity antenna (a) ECC (b) DG (c) TARC (d) CCL.

antenna is placed in the broadside direction at a 5 mm distance from the model for maximum power penetration. The differences in the local and average SAR values are detected in the female breast model at 1W incident power on 1 g tissues with an 8 mm tumor radius. The average and local (maximum and minimum) SAR (W/Kg) of the skin, fat, glandular, and tumor cell are depicted in Table 3. The analysis focuses on two major outcomes, according to the first finding, where the difference between the local and average of SAR are achieved with and without the tumor tissue, which can be analyzed in the practical situation with the tumor-affected breast and normal breast. In the second finding, there is a significant difference in the SAR of the tumor tissue and surrounding glandular tissue, so that the tumor tissue can be easily detected from the breast. The local

https://doi.org/10.1017/S1759078722000332 Published online by Cambridge University Press

Table 3. SAR(average) and SAR(Local)Values of Tissue types at 3.8 GHz

		$SAR_{(average)}$		$SAR_{(Local)}$	
		With Tumor	Without Tumor	With Tumor	Without Tumor
Skin	Max	10.72	10.89	17.76	18.50
	Min	0.0158	0.0165	0.0014	0.00202
Breast Fat	Max	15.50	18.14	27.53	27.90
	Min	0.0020	0.00212	0.0025	0.00214
Glandular Cell	Max	5.12	27.90	10.09	14.12
	Min	0.023	0.00214	0.0018	0.00129
Tumor Cell	Max	16.63	–	47.95	–
	Min	11.40	–	1.73	–

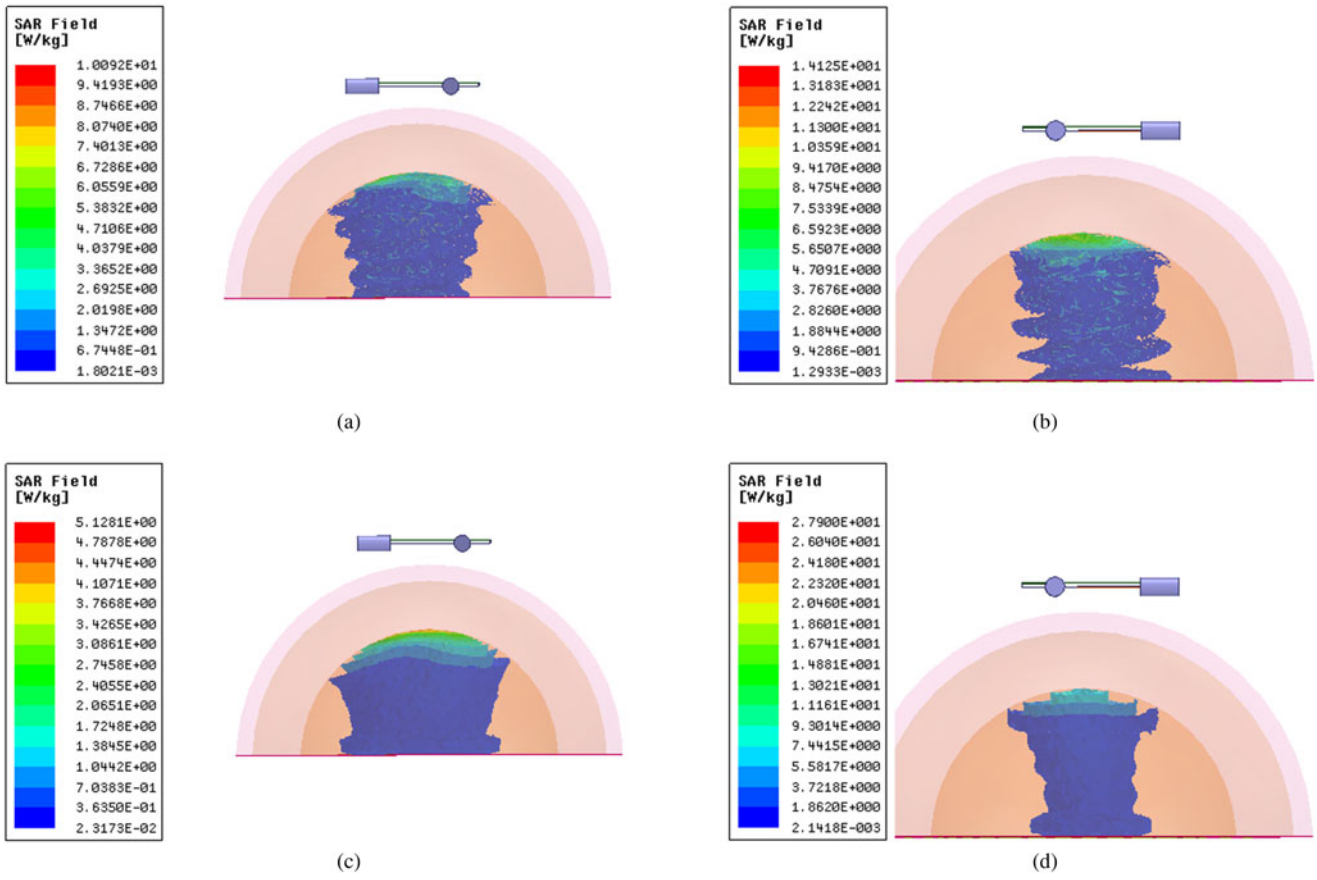

Fig. 5. Analysis of female breast model at 1W power on glandular tissue (a) local SAR with tumor (b) local SAR without tumor (c) average SAR with tumor (d) average SAR without tumor.

and average SAR with and without tumor is illustrated in Fig. 5. The analysis reveals that the proposed two-port antenna can be used in biomedical cancer detection applications.

Conclusion

The two-element circularly polarized textile antenna is presented for 5G, wearable, and biomedical applications. The isolation ($|S_{21}|$) between radiators is enhanced by open slots and diagonal stubs in the ground whereas defected ground perturbs the surface current and is responsible for full band CP. The polarization diversity of orthogonally placed radiators is investigated where ECC and DG are under acceptable limits. The antenna operating bandwidth ($|S_{11}|$) covers the 5G n47, n77, and n78 bands where its application can be found for wearable and cancer detection. The two-port MIMO antenna can be modified further in the eight-port and sixteen-port MIMO antenna for future work with compact size.

Conflict of interest. The author(s) declare none.

https://doi.org/10.1017/S1759078722000332 Published online by Cambridge University Press

References

1. **Zhao B, Mao J, Zhao J, Yang H and Lian Y** (2020) The role and challenges of body channel communication in wearable flexible electronics. *IEEE Transactions on Biomedical Circuits and Systems* **14**, 283–296.
2. **Dicandia FA, Genovesi S and Monorchio A** (2017) Analysis of the performance enhancement of MIMO systems employing circular polarization. *IEEE Transactions on Antennas and Propagation* **65**, 4824–4835.
3. **Kumar A** (2021) Compact 4×4 CPW-fed MIMO antenna with Wi-Fi and WLAN notch for UWB applications. *Radioelectronics and Communications Systems* **64**, 92–98.
4. **Bhattacharjee S, Midya M, Chaudhuri SRB and Mitra M** (2018) Design of a miniaturized dual-band textile antenna using characteristic modal analysis for on-body applications. *Journal of Electromagnetic Waves and Applications* **32**, 2415–2430.
5. **Ashyap AY, Abidin ZZ, Dahlan SH, Majid HA, Waddah AMA, Kamarudin MR, Oguntala GA, Abd-Alhameed RA and Noras JM** (2018) Inverted E-shaped wearable textile antenna for medical applications. *IEEE Access* **6**, 35214–35222.
6. **Arif A, Zubair M, Ali M, Khan MU and Mehmood MQ** (2019) A compact, low-profile fractal antenna for wearable on-body WBAN applications. *IEEE Antennas and Wireless Propagation Letters* **18**, 981–985.
7. **Biswas AK and Chakraborty U** (2019) A compact wide band textile MIMO antenna with very low mutual coupling for wearable applications. *International Journal of RF and Microwave Computer-Aided Engineering* **29**, e21769.
8. **Biswas AK and Chakraborty U** (2020) Reconfigurable wide band wearable multiple input multiple output antenna with hanging resonator. *Microwave and Optical Technology Letters* **62**, 1352–1359.
9. **Singh H, Kanaujia BK, Kumar A, Srivastava K and Kumar S** (2020) Wideband textile multiple-input-multiple-output antenna for industrial, scientific and medical (ISM)/wearable applications. *International Journal of RF and Microwave Computer-Aided Engineering* **30**, e22451.
10. **Dey AB, Pattanayak SS, Mitra D and Arif W** (2021) Investigation and design of enhanced decoupled UWB MIMO antenna for wearable applications. *Microwave and Optical Technology Letters* **63**, 845–861.
11. **Gupta A, Kansal A and Chawla P** (2021) Design of a wearable MIMO antenna deployed with an inverted U-shaped ground stub for diversity performance enhancement. *International Journal of Microwave and Wireless Technologies* **13**, 76–86.
12. **Roy S, Ghosh S, Pattanayak SS and Chakarborty U** (2020) Dual-polarized textile-based two/four element MIMO antenna with improved isolation for dual wideband application. *International Journal of RF and Microwave Computer-Aided Engineering* **30**, e22292.
13. **Haerinia M and Noghanian S** (2019) A printed wearable dual-band antenna for wireless power transfer. *Sensors* **19**, 1732.
14. **Ahmed S, Tahir FA, Shamim A and Cheema HM** (2015) A compact Kapton-based inkjet-printed multiband antenna for flexible wireless devices. *IEEE Antennas and Wireless Propagation Letters* **14**, 1802–1805.
15. nst. of Appl. Phys., Italian Nat. Res. Council, Calculation of the dielectric properties of body tissues in the frequency range 10–100 GHz. Florence, Italy. [Online]. Available at: http://niremf.ifac.cnr.it/tissprop/.
16. **Jha P, Kumar A, De A and Jain RK** (2021) Modified CSRR based dual-band four-element MIMO antenna for 5G smartphone communication. *Progress in Electromagnetics Research Letters* **101**, 35–42.

Anubhav Kumar received B. Tech and M.Tech from Uttar Pradesh Technical University (Now Dr. APJ AKTU), Lucknow, India, in electronics and communication engineering (ECE). He has more than 10 years of teaching experience. He is currently pursuing Ph.D from Shobhit Institute of Engineering and Technology, (Deemed to be University), Meerut, Uttar Pradesh, India. He has published many SCIE/ESCI and Scopus indexed research papers in international journals. His research interests include microstrip antenna, metamaterial, FSS, MIMO antenna, wearable, EBG antenna and image processing.

Professor Asok De was born in November 1955 at Kolkata. He did his B.Tech, M.Tech from Jadavpur University, Kolkata and Ph.D from Indian Institute of Technology, Kharagpur. He served as faculty at the University of Delhi, the University of Kolkata from 1984 to 1997. He joined as a professor of electronics and communication engineering at Delhi College of Engineering (At present Delhi Technological University) in the year 1997. He was the founder principal of Ambedkar Institute of Advanced Communication Technology and Research (2005–2012). He served National Institute of Technology Patna as Director from 2012 to 2017. He also served National Institute of Technology Durgapur as Director (Additional Charge) from 2015 to 2017. Professor De has published more than 200 research papers in international journals and international conferences. He supervised 16 Ph.D scholars. At present, he is an emeritus professor at Delhi Technological University.

Dr. R.K. Jain is a professor & associate dean of the School of Engineering & Technology at Shobhit Institute of Engineering and Technology (Deemed to-be University), Meerut, where he has been teaching and doing research with the collaboration of BHU, Varanasi and BARC, Mumbai. Prof. R.K. Jain obtained his Ph.D. degree from the number one rated university of India, the Banaras Hindu University in 1990. He holds an all-through good academic record. After a brief period of SRA at GNDU, Amritsar, he got an opportunity of post-doctoral fellowship under TRIL program, Trieste in Rome from November, 1997 to July 2001. He worked on cosmic radiation and calculated the radiation doses at different altitudes using passive detectors at ANPA (National Agency for Environmental Protection), Rome. He also worked as postdoctoral fellow at Seoul National University, Seoul, S. Korea from August, 2001 to April, 2002 and was involved in "Dark Matter Search" project. He has also got postdoctoral fellowship at the Department of Physics, North Carolina State University, Raleigh, USA from May, 2002 to June, 2003 and worked on low intensity and low-energy proton beams for the development of low-energy proton detectors (needed to detect protons emitted in neutron beta decay). He has been awarded Confederation of Education Excellence (CEE) Teacher's Award 2014 in recognition of outstanding contribution "No. of National/International/Journals Published". The function was held on 6 September 2014 at Crowne Plaza, Rohini, New Delhi. He has nearly 23 years teaching experience and 30 years of research after Ph.D.

https://doi.org/10.1017/S1759078722000332 Published online by Cambridge University Press